2 Computational Methodology

To examine the catalytic performance of a catalyst for a particular reaction, it is of foremost significance to get exact information about the energetics and strength and nature of interaction of reactant and product molecules with the catalyst. By analysing the electronic structure of the system, one can extract the above information and study the system for particular application. The advancements in theoretical models and computational tools with some approximations, has aided greatly in determining the electronic structure and finding the energetics of a catalytic system to a desirable level of accuracy with reasonable computational cost. In this chapter, we will briefly discuss the formulation of theory employed in the computational model used for geometry optimization and computation of electronic structure in order to understand the catalytic properties of the considered systems in this work. We commence with the basic expressions of the Kohn-Sham method, which form the basis of density functional theory and are utilised in our calculations utilising Quantum ESPRESSO code. Additionally, we will briefly go over a few models and methods, such as the spin polarised d-band model for understanding the activity of transition metals and the climbing-image nudged elastic band (CI-NEB) approach for calculating the activation energy and minimum energy path of a reaction.

2.1 Many-body Problem

Simple quantum systems like the hydrogen atom can now be effectively described by the development of quantum theory using theoretical tools like the time-independent Schrödinger equation (presented in Eq. 2.1 where, $\hat{H}$ is the hamiltonian of the system, $\psi(\vec{F})$ is the single particle eigen function and E is the corresponding eigen value)[1]. The hydrogen atom system is the most basic toy

model; it is a two-body system with a single proton and electron. By using variable separable techniques, it is possible to numerically compute the exact solution of the Schrödinger equation and determine the ground state energy, which is -13.6 eV. However, when a system gets larger-like in the case of the helium-atom, the Schrödinger equation becomes more difficult to solve because there are more variables involved in these many-body systems. This makes determining the precise numerical solution a difficult task, but it can be solved by splitting the system into a two-body system with a reduced mass.

$$-\frac{\hbar^2}{2m}\hat{A}\psi(\vec{r}) = E\psi(\vec{r}) \tag{2.1}$$

In solids, which are thought of as many-electron systems with indistinguishable mutual interactions in a smeared-out background positive nuclear charge, the complexity, however, increases exponentially when we take into account the periodic arrangement of atoms. The 'N particle eigen function describes such a system $\psi\left(\vec{r}_1, \vec{r}_2, \vec{r}_3, \ldots, \vec{r}_N\right)$[2]. Finding the precise solution to a complex many-body system is nearly impossible, as demonstrated by the case of the hydrogen atom. Furthermore, in these large systems, we also encounter complicated interactions between electrons and ions as well as between electrons and electrons, which contributes to the complexity of the system's Hamiltonian, as shown in Eq. 2.2. Here, $\hat{T}_e, \hat{T}_n, \hat{V}_{e,e}, \hat{V}_{e,n}$ and $\hat{V}_{n,n}$ are, the kinetic and potential energy operators (accuonting for electron-electron, electron-ion and ion-ion interactions) respectively[3, 4].

$$\hat{H} = \hat{T}_e + \hat{T}_n + \hat{V}_{e,e} + \hat{V}_{e,n} + \hat{V}_{n,n} \tag{2.2}$$

Considering above equation, the time-dependent, many-body Shcrödinger equation reduces to Eq. 2.3 where, the indices i and k run over the electrons and ions, m_e and m_n are mass of electrons and ions, Z_k and $Z_{k'}$ are the nuclear charge on ions, $\left|\vec{r}_{n,k} - \vec{r}_{n,k'}\right|, \left|\vec{r}_i - \vec{r}_j\right|$ and $\left|\vec{r}_i - \vec{r}_{n,k}\right|$ are the radial distances between ion-ion, electron-electron and electron-ion respectively.

$$-\frac{\hbar^2}{2m}\hat{H}\psi(\vec{r}) = \left(-\frac{\hbar^2}{2m_e}\sum_i \frac{\partial^2}{\partial \vec{r}_i^2} - \frac{\hbar^2}{2m_n}\sum_k \frac{\partial^2}{\partial \vec{r}_{n,k}^2} + \frac{1}{2}\sum_{\substack{k,k' \\ k\neq k'}} \frac{e^2}{4\pi\epsilon_0}\frac{Z_k Z_{k'}}{\left|\vec{r}_{n,k} - \vec{r}_{n,k'}\right|} + \right.$$
$$\left. \frac{1}{2}\sum_{\substack{i,j \\ i\neq j}} \frac{e^2}{4\pi\epsilon_0}\frac{1}{\left|\vec{r}_i - \vec{r}_j\right|} + \sum_i\sum_k \frac{e^2}{4\pi\varepsilon_0}\frac{Z_k}{\left|\vec{r}_i - \vec{r}_{n,k}\right|}\right)\psi(\vec{r}) = E\psi(\vec{r}) \tag{2.3}$$

Since the answer to Eq. 2.3 depends on the atomic mass and charge of the electrons and ions, solving it provides information about the system's ground state in terms of energy eigen values. This method is referred to as first-principles because it eliminates the need for parametric fitting, which is necessary when solving an empirical problem. Nevertheless, the related intricacies continue to exist, rendering the solution of Eq. 2.3 unattainable for a multi-body system. Born and Oppenheimer attempted to solve this problem and bring the equation into solvable form.

2.2 Eigen Function Based Approximations

2.2.1 Born-Oppenheimer Approach

To give you an idea, picture yourself driving a car down a four-lane highway. You can go quicker and pass a number of large vehicles, such trucks and rollers, etc. Therefore, the impact of slow-moving heavy vehicles can be ignored when examining the speed of cars in such a situation. In a similar vein, in a situation where ions and electrons are both contained in a momentum space, the ions would be less mobile than the electrons due to mass. Thus, the Born-Oppenheimer approximation allows us to ignore the ionic contribution in the Hamiltonian given in Eq 2.2[5]. Because of this, it is supposed that the electrons travel in a background of positive charge that is smeared out and comes from the ions that are comparatively static. Consequently, as Eq. 2.4 makes clear, the eigen functions can be expressed as a mixture of the electronic and ionic eigen functions, where, $\chi_k\left(\vec{r}_n\right)$ and $\phi_i\left(\vec{r}_i, \vec{r}_n\right)$ are the ionic and electronic eigen functions respectively.

$$\psi(\vec{r}) = \chi_k\left(\vec{r}_n\right)\phi_i\left(\vec{r}_i, \vec{r}_n\right) \tag{2.4}$$

Then the Eq. 2.3 can be written in variable separated form as shown in Eq. 2.5 and Eq. 2.6 below,

$$\left(-\frac{\hbar^2}{2m_n}\sum_k \frac{\partial^2}{\partial \vec{r}_{n,k}^2} + \frac{1}{2}\sum_{\substack{k,k' \\ k\neq k'}} \frac{e^2}{4\pi\varepsilon_0}\frac{Z_k Z_{k'}}{|\vec{r}_{n,k} - \vec{r}_{n,k'}|}\right)\chi_k(\vec{r}_n) = E_{\chi_k}(\vec{r}_n) \tag{2.5}$$

$$\left(-\frac{\hbar^2}{2m_e}\sum_i \frac{\partial^2}{\partial \vec{r}_i^2} + \frac{1}{2}\sum_{\substack{i,j \\ i\neq j}} \frac{e^2}{4\pi\epsilon_0}\frac{1}{|\vec{r}_i - \vec{r}_j|} + \sum_i\sum_k \frac{e^2}{4\pi\varepsilon_0}\frac{Z_k}{|\vec{r}_i - \vec{r}_{n,k}|}\right)\phi_i(\vec{r}_i, \vec{r}_n) = E\phi(\vec{r}_i, \vec{r}_n) \tag{2.6}$$

Considering Born-Oppenheimer approximation, the first term of Eq. 2.5 vanishes, yielding a constant (β)[6]. Then, the revised Hamiltonian can be rewritten as in Eq. 2.7 where, $\hat{r}_e = -\frac{\hbar^2}{2m_e}\sum_i \frac{\partial^2}{\partial \vec{r}_i^2}$ is the electron kinetic energy operator, $\hat{V}_{e,e} = \frac{1}{2}\sum_{i\neq j}\frac{e^2}{4\pi\varepsilon_0}\frac{1}{|\vec{r}_i - \vec{r}_j|}$ is the electron-electron interaction potential, $\hat{V}_{e,n} = \sum_i\sum_k \frac{e^2}{4\pi\varepsilon_0}\frac{Z_k}{|\vec{r}_i - \vec{r}_{n,k}|}$ is the electron-ion interaction potential and $\beta = \frac{1}{2}\sum_{\substack{k,k' \\ k\neq k'}} \frac{e^2}{4\pi\varepsilon_0}\frac{Z_k Z_{k'}}{|\vec{r}_{n,k'} - \vec{r}_{n,k'}|}$ is an external potential $\left(\hat{V}_{ex}\right)$. From this, the Shcrödinger equation then reduces to the form presented in Eq. 2.8

$$\hat{H} = \hat{T}_e + \hat{V}_{e,e} + \hat{V}_{e,n} + \beta \tag{2.7}$$

$$-\frac{\hbar^2}{2m}\hat{H}\phi(\vec{r}) = \left(-\frac{\hbar^2}{2m_e}\sum_i \frac{\partial^2}{\partial \vec{r}_i^2} + \frac{1}{2}\sum_{\substack{i,j \\ i\neq j}} \frac{e^2}{4\pi\epsilon_0}\frac{1}{|\vec{r}_i - \vec{r}_j|} + \hat{V}_{e,n} + \hat{V}_{ext}\right)\phi(\vec{r}) = E\phi(\vec{r}) \tag{2.8}$$

Given that it ignores the electron-electron interactions, asymmetry, and correlations that govern fermions like electrons, this approximation helps to partially solve the many-body Schrödinger equation's complexity. The Hartree and Hartree-Fock approximations were used to address this issue.

2.2.2 Hartree Approach

To further simplify the many-body problem, the coulomb interactions between electrons governed by classical electrostatics had to be addressed. This was accomplished by Hartree, who transformed the many-body problem into the independent electron approximation, or one-electron issue[7–10]. As in Eq. 2.9, the electron-electron interaction potential that contributes to the Hamiltonian shown

in Eq. 2.7 can be expressed in terms of the charge density ρ(r), independent of the self-interactions.

$$\hat{V}_{e,e}(r) = \int \frac{[\rho\,(r') - \rho_i\,(r')]}{|r - r'|} dr' \tag{2.9}$$

Classical electrostatics states that the electrostatic potential V_l(r) is determined by the Poisson's relation, which is given in Eq. 2.10. It is derived from the distribution of electronic charge density in space, ρ(r). The potential energy of the electrons in such an electrostatic potential is called the Hartree potential V_H(r), and it satisfies Poisson's relation and transforms in Hartree units as $V_H(\mathbf{r}) = -V_l(\mathbf{r})$.

$$\nabla^2 V_l(r) = \frac{\rho(r)}{\epsilon_0} \tag{2.10}$$

The individual eigen states can then be summed as follows, with the summation extending across all of the occupied eigen states, to produce the electronic charge distribution that corresponds to the Hartree potential;

$$\rho(r) = \sum_m |\psi_m(r)|^2 \tag{2.11}$$

This results in the conversion of the electron-electron interaction potential to the single electron potential, or Hartree potential, as given in Eq. 2.13 (by applying Eq. 2.11 in Eq. 2.9).

$$\hat{V}_{e,e}(r) = V_l(r) = \sum_{m \neq 1} \int \frac{|\psi_m(r)|^2}{|r - r'|} dr' \tag{2.12}$$

Additionally, Hartree proposed that the many-body eigen function be expressed as the product of the eigen functions of each individual electron that makes up the system, as seen in the following Eq. 2.13.

$$\psi\,(\vec{r}_1, \vec{r}_2, \ldots, \vec{r}_N) = \prod_{m=1}^{N} \psi\,(\vec{r}_m) \tag{2.13}$$

Next, we obtain the modified Schrödinger equation (Eq. 2.14) also referred to as the Hartree equation, by introducing the Hartree potential given in Eq. 2.12 in Eq. 2.8.

$$\left(-\frac{\hbar^2}{2m_e} \sum_i \frac{\partial^2}{\partial \vec{r}_i^2} + \sum_{m \neq 1} \int \frac{|\psi_m(r)|^2}{|r - r'|} dr' + \hat{V}_{e,n} + \hat{V}_{ext} \right) \psi(\vec{r}) = E\psi(\vec{r}) \tag{2.14}$$

However, the electronic correlations were not incorporated by Hartree and this missing piece led to the Hartree-Fock approximations[11, 12].

2.2.3 Hartree-Fock Approach

The two main issues with the Hartree approach were that (i) the electron-electron interactions were averaged and (ii) the electron eigen functions were not anti-symmetric with regard to electron exchange. The former issue is handled by the Hartree-Fock approach (which was pointed out by Slater and Fock independently) [13, 14]. They started with an anti-symmetric eigen function as a function of location and spin (shown in Eq. 2.15 below), which complies with the Pauli exclusion principle, which states that eigen functions must be anti-symmetric under particle exchange. Because of this, no two electrons can have the same set of quantum numbers, meaning that two electrons with the same spin cannot occupy the same eigen state at the same time.

$$\psi_{HF}\left[\left(\vec{r}_1,\sigma_1\right),\left(\vec{r}_2,\sigma_2\right),\ldots,\left(\vec{r}_N,\sigma_N\right)\right]=-\psi_{HF}\left[\left(\vec{r}_1,\sigma_1\right),\left(\vec{r}_2,\sigma_2\right),\ldots,\left(\vec{r}_N,\sigma_N\right)\right] \tag{2.15}$$

Additionally, in place of the product of eigen functions given in Eq. 2.13, we employ a Slater determinant eigen function, which fulfils anti-symmetry and is stated in Eq. 2.16 where $\boldsymbol{\psi}_r\left(\vec{r}_s,\sigma_s\right)$ are one electron eigen functions.

$$s=\frac{1}{\sqrt{N!}}\begin{vmatrix}\psi_1\left(\vec{r}_1,\sigma_1\right) & \psi_1\left(\vec{r}_2,\sigma_2\right) & \ldots & \psi_1\left(\vec{r}_N,\sigma_N\right)\\ \psi_2\left(\vec{r}_1,\sigma_1\right) & \psi_2\left(\vec{r}_2,\sigma_2\right) & \ldots & \psi_2\left(\vec{r}_N,\sigma_N\right)\\ \vdots & \vdots & \ldots & \vdots\\ \psi_N\left(\vec{r}_1,\sigma_1\right) & \psi_N\left(\vec{r}_2,\sigma_2\right) & \ldots & \psi_N\left(\vec{r}_N,\sigma_N\right)\end{vmatrix} \tag{2.16}$$

Next, as in Eq. 2.14, we minimise the expected value of the Hamiltonian by applying the Lagrangian multiplier approach, which leads us to the set of Hartree-Fock equations shown in Eq. 2.17, where s_m and s_l are spin labels. While the electron exchange is taken into consideration, this method is computationally costly because it necessitates the minimising of the "N particle Slater determinant" in

order to get the total energy of the system E in Eq. 2.17.

$$\left(-\frac{\hbar^2}{2m_e}\sum_i \frac{\partial^2}{\partial \vec{r}_i^2} + \hat{V}_{e,n} + \hat{V}_{exi} + \sum_{m\neq 1}\int \frac{|\psi_m(r)|^2}{|r-r'|}dr' - \sum_m \delta_{s_m,s_1}\int \frac{\psi_m^*(r')\,\psi_1(r')}{|r-r'|}dr'\right)\psi(\vec{r}) = E\psi(\vec{r}) \tag{2.17}$$

Because there would be 3N degrees of freedom for a system with N electrons, increasing the number of variables in the issue, the many-body Schrödinger equation is complex. This problem is solved by density functional theory, which approximates the many-body problem to a single computationally feasible electronic density.

2.3 Density Based Approximations

2.3.1 Thomas-Fermi Approach

Thomas and Fermi suggested that instead of taking into account the single particle eigen functions suggested by Hartree and Hartree-Fock methods[15, 16], the overall energy of a system can be expressed as a functional of the electron density. Consequently, the electron density (n($\vec{r}$)) can be used to express the kinetic energy of a set of 'N' interacting electrons, as shown in Eq. 2. 18. As in Eq. 2. 19, where the kinetic energy, electrostatic energy, and external potential are expressed as a functional of electron density, the total energy (E) can then be defined as a functional of electron density.

$$T_{rF} = C_k \int n(\vec{r})^{5/3} d^3r \tag{2.18}$$

$$E = C_k \int n(\vec{r})^{5/3} d^3r + \int \hat{V}_{ext}(\vec{r}) n(\vec{r}) + \frac{1}{2}\iint \frac{e^2}{4\pi\epsilon_0}\frac{n(\vec{r}')\,n(\vec{r})}{|r-r'|} d^3r d^3r' \tag{2.19}$$

The aforementioned equation can then be minimised by continuing with the Lagrangian multiplier approach[17]. One disadvantage of this strategy is that it leaves out the electron exchange. Dirac addressed issue by introducing the correlation functional and exchange interaction, but he was unable to determine the shell structure or the behaviour of atoms in complicated systems[18, 19].

2.3.2 Hohenberg-Kohn Approach

The foundation of density functional theory was established by two theorems developed by Hohenberg and Kohn[20]. Below is a statement of the two theorems.
Theorem I:
"The external potential $\hat{V}_{ext}(\vec{r})$, and hence the total energy, is a unique functional of the electron density $n(\vec{r})$."
The above-mentioned theorem's energy functional can be written in terms of the external potential as shown in Eq. 2.20, where, F[n($\vec{r}$)] is an unknown universal functional of the electron density $\mathbf{n}(\vec{r})$.

$$E[n(\vec{r})] = \int \hat{V}_{ex(}(\vec{r})n(\vec{r})dr + F[n(\vec{r})] \tag{2.20}$$

$$E[n(\vec{r})] = \langle\psi|\hat{H}|\psi\rangle \tag{2.21}$$

Assuming the existence of a non-degenerate ground state, the system's ground state can be determined by designing a Hamiltonian (Eq. 2.22) that corresponds to the total energy functional (Eq. 2.20). This is done by ensuring that the eigen function minimises the expectation value (Eq. 2.21).

$$\hat{H} = \hat{F} + \hat{V}_{\text{ext}} \tag{2.22}$$

$$\hat{F} = \hat{T}_e + \hat{V}_{e,e} \tag{2.23}$$

where the electron-electron interaction potential and kinetic energy, as shown in Eq. 2.23, comprise the electronic Hamiltonian $\hat{\boldsymbol{F}}$. This is the same for all N' electron systems where the external potential $\hat{V}_{\text{exi}}$ ($\vec{r}$) and "N" electrons fully characterise the Hamiltonian.
Take into consideration ${}^1\hat{V}_{\text{ext}}$ ($\vec{r}$) and ${}^2\hat{V}_{\text{ex }1}(\vec{r})$, two distinct external potentials that would produce the same electron density n($\vec{r}$). After then, the related Hamiltonians ${}^1\hat{H}$ and ${}^2\hat{H}$ would result in distinct ground states, ${}^1\psi$ and ${}^2\psi$, respectively, with an associated electron density of $\mathbf{n}(\vec{r})$. Following that, we obtain; using the variational principle and Eq. 2.23

$$\begin{aligned} {}^1E_0 \left\langle \left\langle {}^2\psi \right|^1 \hat{H} \mid {}^2\psi \right\rangle &= \left\langle {}^2\psi \right|^2 \hat{H} \mid {}^2\psi \Big\rangle + \left\langle {}^2\Psi \left| {}^1\hat{H} - {}^2\hat{H} \right|^2 \psi \right\rangle \\ &= {}^2E_0 + \int n(\vec{r}) \left[{}^1\hat{V}_{ext}(\vec{r}) - {}^2\hat{V}_{ext}(\vec{r}) \right] dr \end{aligned} \tag{2.24}$$

$$^2E_0 < {}^1E_0 + \int n(\vec{r}) \left[{}^1\hat{V}_{ext}(\vec{r}) - {}^2\hat{V}_{ext}(\vec{r}) \right] dr \tag{2.25}$$

$$^1E_0 + {}^2E_0 < {}^2E_0 + {}^1E_0 \tag{2.26}$$

Where, $^1\mathrm{E}_0$ and $^2\mathrm{E}_0$ are the ground state energies corresponding to the Hamiltonians $^1\hat{\boldsymbol{H}}$ and $^2\hat{\boldsymbol{H}}$ respectively. By adding Eq. 2.24 and Eq. 2.25 we get Eq. 2.26 which is in contradiction to our assumptions and proves that, there can be only one external potential $\hat{V}_{\mathrm{ext}}$ which uniquely determines the ground state density $\mathrm{n}(\vec{r})$ and vice-versa.

Theorem II:

"The groundstate energy can be obtained variationally: the density that minimises the total energy is the exact groundstate density."

The Hamiltonian $\hat{H}$ governs the eigenfunctions of a system of 'N' particles, which is determined by the external potential $\hat{V}_{\mathrm{ext}}$ and the number of particles. Moreover, theorem I makes it clear that the external potential is determined by the electron density $\mathrm{n}(\vec{r})$. This suggests that, the expectation value of $\hat{F}$ is likewise a functional of the electron density $\mathrm{n}(\vec{r})$, as the eigen function is a functional of the electron density $\mathrm{n}(\vec{r})$, as shown by Eq. 2.27.

$$F[n(\vec{r})] = \langle \psi | \hat{F} | \psi \rangle \tag{2.27}$$

Let us consider an energy functional $\mathrm{E_x}[\mathrm{n}(\vec{r})]$ wherein the external potential $\hat{V}_{\mathrm{ext}}$ is independent of an unknown electron density $\mathrm{n}'(\vec{r})$ as presented in Eq. 2.28.

$$E_x[n(\vec{r})] = \int \hat{V}_{ext}(\vec{r}) n'(\vec{r}) dr + F\left[n'(\vec{r})\right] \tag{2.28}$$

Then, in accordance to the variational principle,

$$\left\langle \psi' | \hat{F} | \psi' \right\rangle + \left\langle \psi' \left| \hat{V}_{ext}(\vec{r}) \right| \psi' \right\rangle \left\langle \psi | \hat{F} | \psi \right\rangle + \left\langle \psi \left| \hat{V}_{ext}(\vec{r}) \right| \psi \right\rangle \tag{2.29}$$

Where, ψ is the eigen function corresponding to the correct ground state electron density $\mathbf{n}(\vec{r})$. We get;

$$\int n'(\vec{r}) \hat{V}_{ext}(\vec{r}) dr + F\left[n'(\vec{r})\right] > \int n(\vec{r}) \hat{V}_{ext}(\vec{r}) dr + F[n(\vec{r})] \tag{2.30}$$

Then, according to the variational principle we reach at;

$$E_x\left[n'(\vec{r})\right] > E_x[n(\vec{r})] \tag{2.31}$$

The ground state energy and matching electron density, $n(\vec{r})$, are therefore implied to be lower than any other electron densities, $\mathrm{n}'(\vec{r})$. This variational concept is called the Hohenberg-Kohn theorem. It states that if and only if the input electron density equals the genuine ground state electron density $n(\vec{r})$, then the universal functional $\hat{F}[n(\vec{r})]$ produces the lowest energy state.

2.3.3 Kohn-Sham Approach

Density Functional Theory was developed as a useful tool to determine a system's ground state by the Kohn-Sham method[21]. This method uses Eq. 2.32 to parametrize the electron density $n(\vec{r})$ into a single electron orbital $\zeta_1(\vec{r})$, where the summation is over all occupied states, and Eq. 2.33 to describe the total energy functional.

$$n(\vec{r}) = \sum_i \zeta_1^*(\vec{r})\zeta_1(\vec{r}) \tag{2.32}$$

$$E[n(\vec{r})] = T[n(\vec{r})] + E_H[n(\vec{r})] + E_{xc}[n(\vec{r})] + E_{ext}[n(\vec{r})] \tag{2.33}$$

Where, E_H is the electron-electron interaction under Hartree approximation, E_{ext} is the external potential and the kinetic energy of the non-interacting electrons in $\zeta_1(\vec{r})$ are given as;

$$E_H[n(\vec{r})] = \iint \frac{n(\vec{r})n\left(\vec{r}'\right)}{|\vec{r} - \vec{r}'|} dr dr' \tag{2.34}$$

$$E_{ext}[n(\vec{r})] = \int \hat{V}_{exi} n(\vec{r}) dr \tag{2.35}$$

$$T[n(\vec{r})] = \sum_i \int \zeta_i^*(\vec{r}) \left(-\frac{1}{2}\nabla^2\right) \zeta_i(\vec{r}) d^3r \tag{2.36}$$

The remaining quantity in Eq. 2.33 is known as the exchange-correlation energy $\mathrm{E}_{xc}[\mathrm{n}(\vec{r})]$. As the single electron orbitals $\zeta_i(\vec{r})$ are variational quantities, the variation of the total energy functional with respect to these orbitals $\zeta_i^*(\vec{r})$ would result into an effective single electron equation known as the Kohn-Sham equation,

presented in Eq. 2.37 below.

$$\left(-\frac{1}{2}\nabla^2 + \int \frac{n\left(\vec{r'}\right)}{|\vec{r}-\vec{r'}|}dr' + \hat{V}_{ext}[n(\vec{r})] + \frac{\delta E_{xc}[n(\vec{r})]}{\delta n(\vec{r})}\right)\zeta_i(\vec{r}) = \epsilon_i\zeta_i(\vec{r}) \tag{2.37}$$

The Kohn-Sham equation for electrons in a potential are given by Eq. 2.38 here, the exchange-correlation potential can be obtained by the variation of exchange-correlation energy as presented in Eq. 2.39.

$$V_{eff}(\vec{r}) = V_{ext}(\vec{r}) + \int \frac{n\left(\vec{r'}\right)}{|\vec{r}-\vec{r'}|}d^3r' + V_{xc}[n(\vec{r})] \tag{2.38}$$

$$V_{xc}[n(\vec{r})] = \frac{\delta E_{xc}[n(\vec{r})]}{\delta n(\vec{r})} \tag{2.39}$$

Thus, the modified form of the Kohn-Sham equation is as follows;

$$\left(-\frac{1}{2}\nabla^2 + V_{eff}(\vec{r})\right)\zeta_i(\vec{r}) = \epsilon_i\zeta_1(\vec{r}) \tag{2.40}$$

Here, $\boldsymbol{\varepsilon}_i$ are the Lagrange parameters introduced to retain the orthogonality of the single-particle Kohn-Sham orbitals as follows;

$$\int \zeta_i^*(\vec{r})\zeta_j(\vec{r})d^3r = \delta_{lJ} \tag{2.41}$$

2.4 Exchange and Correlation Functionals

The Kohi-Sham approach's exchange and correlation functionals specify the precision of computations and results. Numerous functionals have been constructed since the theory's inception with the aim of predicting chemically exact outcomes. In general, they can be categorised and comprehended using the Jacob's ladder, wherein the computational expense rises as one climbs the ladder towards a depiction of the system being studied that is chemically precise. Certain constraints must be met by the exchange and correlation functionals, namely: (i) they must exhibit slowly varying densities and reduce to a homogenous two-dimensional electron gas limit; (ii) they must be asymptotic for atoms and molecules; (i.e.,

$V_{xc}[n(\vec{r})] \rightarrow -\frac{1}{\vec{r}}$ for $\vec{r} \rightarrow \infty$) and (iii) they must not be self-interacting. These functionals fall into one of three categories: non-local, semi-local, or local.

2.4.1 Local Density Approximation

Equations 2.42 and 2.43 offer the local density approximation and local spin-density approximation, respectively[20]. These are referred to as local functionals because the exchange energy functional is dependent on the electron density and spin at a particular point $\vec{r}$ in the atom's electron cloud.

$$E_{xc}^{LDA}[n(\vec{r})] = \int \epsilon_{xc}[n(\vec{r})]n(\vec{r})d^3r \tag{2.42}$$

$$E_{xc}^{LSDA}\left[n_{\uparrow}(\vec{r}), n_{\downarrow}(\vec{r})\right] = \int \epsilon_{xc}\left[n_{\uparrow}(\vec{r}), n_{\downarrow}(\vec{r})\right] n(\vec{r})d^3r \tag{2.43}$$

2.4.2 Generalized Gradient Approximation

Eqs. 2.44 and 2.45 provide the generalised gradient approximation and the generalised spin-gradient approximation, respectively[22, 23]. Since the energy functional at a given point $\vec{r}$ and its neighbourhood depends on the electron density and its gradients, these functionals are referred to as semi-local functionals. PBE is one of the most popular and well-known semi-local functions.

$$E_{xc}^{GGA}[n(\vec{r})] = \int \epsilon_{xc}[n(\vec{r}), \nabla n(\vec{r})]n(\vec{r})d^3r \tag{2.44}$$

$$E_{xc}^{GSGA}\left[n_{\uparrow}(\vec{r}), n_1(\vec{r})\right] = \int \epsilon_{xc}\left[n_{\uparrow}(\vec{r}), n_1(\vec{r}), \nabla n_{\uparrow}(\vec{r}), \nabla n_1(\vec{r})\right] n(\vec{r})d^3r \tag{2.45}$$

After accounting for the kinetic energy densities (as shown in Eq. 2.36) we obtain an additional semi-local functional, the meta-generalized gradient approximation (usually shown as in Eq. 2.46)[24, 25]. In these functionals, we take into account the density Laplacians in addition to the gradients. These functionals are helpful in determining if a system contains a metallic or covalent link, despite the fact that they show divergent behaviour when applied to diatomic systems. TPSS and

SCAN are two functionals that are used often.

$$E_{xc}^{meta-GGA}\left[n_{\uparrow}(\vec{r}), n_{\downarrow}(\vec{r})\right] = \int \epsilon_{xc}\left[n_{\uparrow}(\vec{r}), n_{\downarrow}(\vec{r}), \nabla n_{\uparrow}(\vec{r}), \nabla n_{\downarrow}(\vec{r}), \nabla^2 n_{\uparrow}(\vec{r}), \nabla^2_{\downarrow}(\vec{r})\right] n(\vec{r}) d^3r \tag{2.46}$$

2.4.3 Hybrid Approximation

Despite being more computationally expensive than other approximations, hybrid functionals are a class of non-local functionals that are chosen because they yield chemically accurate results[26]. The energy functional in these functionals is dependent upon the density of orbitals throughout the atom's electron cloud. These functionals have two advantages: (i) we can eliminate the self-interaction term; and (ii) we can obtain the correct asymptotic form i.e., $-\frac{1}{\vec{r}}$ for large $\vec{r}$. Establishing an exchange correlation energy functional as in Equation 2.47 is the straightforward approach. However, there is a mathematical issue with error cancellation in LDA and GGA, meaning that errors in LDA correlation are much greater than errors in exchange, and the faults in LDA exchange are cancelled out. Therefore, the solution is to modify Eq. 2.47 into Eq. 2.48, which takes the form of Eq. 2.49 for the PBE0 functional (one of the earliest hybrid functionals), by adding a mixing parameter ($\alpha; 0 < \alpha < 1$).

$$E_{xc}^{hybrid}[n(\vec{r})] = E_x^{exact}[n(\vec{r})] + E_c^{LDA/GGA}[n(\vec{r})] \tag{2.47}$$

$$E_{xc}^{\text{hybrid}}\left[n(\vec{r})\right] = \alpha E_x^{exact}[n(\vec{r})] + (1-\alpha)E_x^{GGA}[n(\vec{r})] + E_c^{GGA}[n(\vec{r})] \tag{2.48}$$

$$E_{xc}^{\text{hybrid}}\left[n(\vec{r})\right] = \frac{1}{4}E_x^{exact}[n(\vec{r})] + \frac{3}{4}E_x^{GGA}[n(\vec{r})] + E_c^{GGA}[n(\vec{r})] \tag{2.49}$$

2.5 Electronic Approximations

2.5.1 Plane-wave and Pseudopotentials

The basis set, such as a plane wave basis set based on the Blöch theorem (as in Eq. 2.50 below), can be expanded from the Kohn-Sham orbitals used to represent the single particle density. This is appropriate to characterise the electrons in a

periodic potential observed in materials[27]. Furthermore, since the potential is in real space and the kinetic energy operator is diagonal in a plane wave basis set, we can lower the computing cost by converting between the representations using rapid Fourier transforms[28].

$$\psi_{\vec{k}}^{n}(\vec{r}) = \sum_{\vec{k}} c_{\vec{k}}^{n,\vec{k}} e^{l(\vec{k}+\vec{k})\vec{r}} \tag{2.50}$$

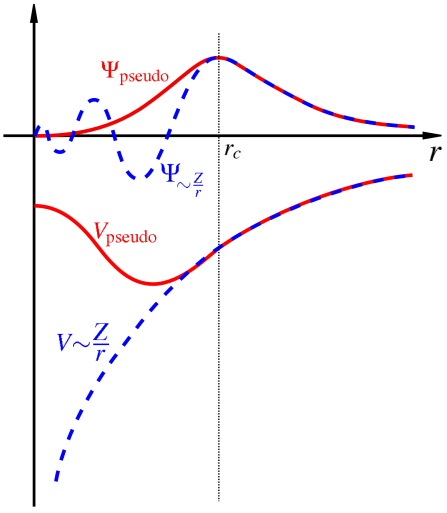

FIGURE 2.1: A schematic representation of pseudopotential. Adopted from Phys. Rev. B., 50, 17953-17979, (1994).

Nevertheless, a plane wave basis set's main drawback is its inefficiency because it would take a huge number of basis sets to describe atomic eigen functions near nucleus. Since the majority of the valence electrons alone are responsible for governing the materials' physical and chemical properties, this challenge is addressed by the use of pseudo-potentials that simulate the potential of the ionic core and the core electrons. This is contingent upon meeting specific requirements, including: (i) valence eigen functions staying constant outside the core region $\mathbf{r}_c$; (ii) the pseudo eigen function inside the core matching precisely at the boundary; and (iii) the pseudo eigen function and its first derivative being continuous at the boundary and (iv) inside the core region, the pseudo eigen function is nodeless. The eigen function of a nucleus's coulomb potential is shown in blue in Fig. 2.1, while the pseudo-eigen function is shown in red[29]. These conditions are graphically represented. The core radius, $\mathbf{r}_c$ is the point beyond which the real and pseudo-eigen

functions, as well as the potentials matches.

$$\psi = \tilde{\psi} + \sum_{1}^{n} c_i \phi_i - \sum_{i}^{n} c_i \tilde{\phi}_i \tag{2.51}$$

Over time, many classes of pseudopotentials have been developed, such as the ultra-soft, norm-conserving, projector-augmented wave technique, and others[30–32]. As an all-electron eigen function with three components, as shown in Eq. 2.51, where $\tilde{\psi}$ is the pseudo eigen function, ϕ_i is the all-electron partial eigen function, and $\tilde{\phi}_i$ is the pseudo partial eigen function, the projector-augmented wave method is particularly an improvement over the original techniques. The pseudo eigen functions in this case are represented by plane waves, which differ considerably from all electron eigen functions in the vicinity of the ionic core but adequately describe the eigen functions in areas far from the ion core. Therefore, to account for this error, the all electron eigen functions are introduced in Eq. 2.51.

2.5.2 van der Waals Corrections

The representation of long-range dispersion forces is not effectively accommodated into the traditional framework of density functional theory's local density approximation or generalised gradient approximation. This is essential in computation of the adsorption characteristics of molecules over surfaces and interfaces. Grimme devised a semiempirical van der Waals correction technique, famously referred to as the D2 and D3 correction, to resolve this problem by precisely including the long-range dispersion forces into the conventional density functional theory[33–35]. The van der Waals correction term (E_{disp}), as shown in Eq. 2.52, is added to the total energy of the Kohn-Sham system (E_{KS}) computed under the self-consistent field theory.

$$E_{DFT+D2/D3} = E_{KS} + E_{disp} \tag{2.52}$$

In the D2 scheme; in addition to Kohn-Sham energy, a semi-empirical dispersion potential (C_6R^{-6}) and damping function (f_{damp}, at small atomic distances) are added in the form of a correction term as presented in Eq. 2.53.

$$E_{disp} = -S_6 \sum_{i=1}^{N_{ej}-1} \sum_{j=i+1}^{N_{ei}} \frac{C_6^{jj}}{R_{ij}^6} f_{dump}\left(R_{ij}\right) \tag{2.53}$$

While, in the D3 scheme, a sum-up of two-body $\left(\mathrm{E}^{(2)}\right)$ and three-body $\left(\mathrm{E}^{(3)}\right)$ energies forming the dispersion correction term $\mathrm{E}_{\mathrm{disp}}$ is incorporated into the Kohn-Sham energy wherein the terms $\left(\mathrm{E}^{(2)}\right)$ and $\left(\mathrm{E}^{(3)}\right)$ are presented in Eq. 2.54 and Eq. 2.55, respectively.

$$E^{(2)} = \sum_{AB} \sum_{\substack{n=2m \\ m=1,2,3,\ldots}} S_n \frac{C_n^{AB}}{r_{AB}^n} f_{d,n}\left(r_{AB}\right) \tag{2.54}$$

$$E^{(3)} = \sum_{ABC} f_{d,(3)}\left(r_{ABC}\right) E^{(ABC)} \tag{2.55}$$

In Eq. 2.53 and Eq. 2.54, the global scaling factors S_n and S_6 are directly dependent on the exchange-correlation functional. This means that for generalised gradient approximation functionals like $PBE; S_6 = 1.00$ and $S_8 = 0.72$ are applicable. For every ' ij ' and 'AB' pair of atoms with interatomic distances of R_{ij} and r_{AB}, respectively, the n^{th} order dispersion coefficients are represented by the equations above by the symbols C_6^{ij} and C_n^{AB}. To prevent singularities at small distances, R_{ij} and r_{AB}, with r_{ABC} serving as the average radius of a triple atom system 'ABC' with $\mathrm{E}^{(\mathrm{ABC})}$ denoting a non-additive triple dipole dispersion term, the damping functions (f_{damp} and $\mathrm{f}_{d,n}$) are incorporated.

2.6 Electronic Properties

Modern computational materials science provides sophisticated tools for analysing the electronic structure and characteristics like density of states, electronic reavtivity descriptors, which plays significant role in understanding catalytic behaviour of the system.

2.6.1 Density of State

Analysis of density of states (DOS) per unit of energy E (and per unit of volume ω in the extended matter) provides valuable insights about various many important

properties of the system,

$$g(E) = \frac{1}{N_k} \sum_i \sum_{\vec{k}} \delta\left(\varepsilon_{i,\vec{k}} - E\right) = \frac{\omega_{\text{cell}}}{(2\pi)^d} \int_{BZ} \delta\left(\varepsilon_{i,\vec{k}} - E\right) d\vec{k} \tag{2.56}$$

When it comes to independent-particle states, $n(E)$ is the number of independent-particle states per unit of energy, where $\varepsilon_{i,\vec{k}}$ is the energy of an electron (or phonon). The computation of the integral in Eq. 2.56 is, in theory, a difficult task. The linear tetrahedron approach (LTM) by Jepsen and Andersen, the modified tetrahedron method (MTM) by Bloch et al., and the Gaussian broadening method (GBM) by Methfessel and Paxton are three common types of methodologies for this Brillouin zone integration that are listed here[36–38]. Fig. 2.2 schematically illustrates the DOS of bulk, 2D, 1D and 0D materials[39].
Eq. 2.56 defines the total density of states which is a projection of all bands of the electronic band structure over all k-points. If one wants to analyze space-resolved DOS in the real space, the local density of states (LDOS) may be defined as

$$g(\vec{r}, E) = \sum_i \sum_{\vec{k}} \left|\psi_{i\vec{k}}(\vec{r})\right|^2 \delta\left(\varepsilon_{i,\vec{k}} - E\right) \tag{2.57}$$

To study the interaction of atoms with each other, we analyze the projected

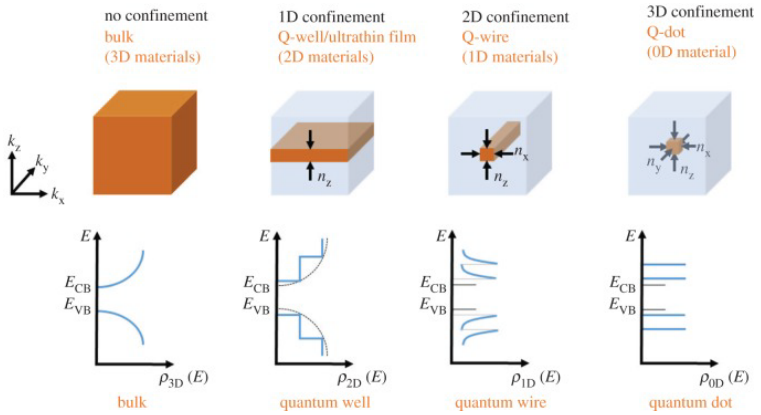

FIGURE 2.2: Schematic illustration of broken symmetry and functional form of the density of states in 1D, 2D, and 3D confined materials.

density of states (PDOS), which is in principle a projection of the DOS onto atomic orbitals, computed as

$$g(\alpha, E) = \sum_i \sum_{\vec{k}} \left|\left\langle \psi_{\alpha\vec{k}}(\vec{r}) \mid \psi_{i\vec{k}}(\vec{r}) \right\rangle\right|^2 \delta\left(\varepsilon_{i,\vec{k}} - E\right) \tag{2.58}$$

where $\psi_{\alpha\vec{k}}$ denotes orthonormal states to $\psi_{i\vec{k}}$.

2.6.2 Electronic Reactivity Descriptors

In examining the catalytic properties of transition-metal (TM) based systems, the analysis of d-orbital of TM plays huge role as the origin of exemplary catalytic behaviour of TMs are their partially filled *d*-orbitals. Moreover, the interaction of the TM-catalyst with substrates or reactants alters the structure of d-orbital, thereby affecting the catalytic performance greatly. In this regard, we employed the spin-polarized *d*-band model for determining the electronic descriptors adduced by Bhattacharjee and co-workers (modification of Nørskov and Hammer *d*-band model), i.e., *d*-band center (ε_d), *d*-band width (W_d) and fractional filling (f_l) of *d*-band (for spin-up and spin-down states) for representative systems using Eq. 2.59, Eq. 2.60 and Eq. 2.61, respectively[40, 41]. The ε_d was computed as the first moment of the density of states projected on the *d* band about the Fermi level (E_F) and is expressed as,

$$\varepsilon_d = \frac{\int_{-\infty}^{E_F} (E - E_F)\, D_{d\sigma}(E) dE}{\int_{-\infty}^{E_F} D_{d\sigma}(E) dE} \tag{2.59}$$

The W_d was computed as the square root of the second moment of the *d*-band density of states projected on the *d*-band about the ε_d and is expressed as,

$$W_d = \frac{\int_{-\infty}^{E_F} D_{d\sigma}(E) \left[(E - E_F) - \varepsilon_d\right]^2 dE}{\int_{-\infty}^{E_F} D_{d\sigma}(E) dE} \tag{2.60}$$

The f_l was taken as the integral overstates up to the Fermi level divided by the integral over all states as,

$$f_l = \frac{\int_{-\infty}^{E_F} D_{d\sigma}(E) dE}{\int_{-\infty}^{\infty} D_{d\sigma}(E) dE} \tag{2.61}$$

Where, $D_{d\sigma}(E)(\sigma = \uparrow, \downarrow)$ is the DOS projected on the d-states of the TM, E is the energy and E_F is the Fermi energy of the system. Figure 2.6 illustrates the schematic of the spin-polarized DOS of the transition metal with the electronic reactivity descriptors.

2.7 Reaction Mechanism Analysis

2.7.1 Regular NEB Method

In order to investigate proficiency of a catalyst towards any reaction, the computation of minimum energy path (MEP) provides a thorough insight about it. Nudged elastic band (NEB) is a computational technique to simulate and perform a chemical reaction and plot a MEP. The NEB method primarily provides us a transition state or saddle point along the reaction path between two states of a system, which rerpesents the highest energy point along the reaction pathway. It works on the concpet of elastic band with $N+1$ images can be denoted by $[\mathrm{R}_0, \mathrm{R}_1, \mathrm{R}_2, \ldots, \mathrm{R}_\mathrm{N}]$, where the end points, R_0 and R_N, are fixed and given by the energy minima corresponding to the initial and final states. The $N-1$ intermediate images are adjusted by the optimization algorithm[42, 43]. In NEB, 'nudged' refers to an iterative process used to optimize the elastic band, i.e., in each iteration, the total force acting on an image which is the sum of the spring force along the local tangent and the true force perpendicular to the local tangent (Eq. 2.62), is optimized, the band is nudged towards the direction of lower energy/force along the reaction path, while maintaining the elasticity.

$$F_i = F_i^s|_{\|} - \nabla E\left(R_i\right)|_{\perp} \tag{2.62}$$

where the true force is given by

$$\nabla E\left(R_i\right)|_{\perp} = \nabla E\left(R_i\right) - \nabla E\left(R_i\right) \cdot \hat{\tau}_i \tag{2.63}$$

Here, E is the energy of the system, a function of all the atomic coordinates, and $\hat{\tau}_i$ is the normalized local tangent at image i. The spring force is

$$F_i^s|\,\| = k\left(|Ri+1-R_i| - |R_i - R_{i-1}|\right) \cdot \hat{\tau}_i \tag{2.64}$$

where k is spring constant. Each image converges to MEP by iteratively solving Eq. 2.62. But the limitation of NEB is that none of the image falls on the saddle point (as shown in Fig. 2.3) which makes it difficult to estimate the energy of saddle point as it needs to be done by interpolation.

2.7.2 Climbing Image NEB Method

The NEB method has been slightly modified by the climbing image NEB (CI-NEB) method[44]. Here, although the shape of the MEP is preserved but a rigorous convergence to a saddle point achieved with no appreciable increase in computational efforts. This additional Here, after few iterations of regular NEB, the image with the highest energy i_{max} is identified and the force on this one image is not then optimized using Eq. 2.62 but rather,

$$F_{i_{\max}} = -\nabla E\left(R_{i_{\max}}\right) + 2\nabla E\left(R_{i_{\max}}\right)|\,\| = -\nabla E\left(Ri_{\max}\right) + 2\nabla E\left(R_{i_{\max}}\right)\cdot\hat{\tau}_{i_{\max}}\hat{\tau}_{i_{\max}} \tag{2.65}$$

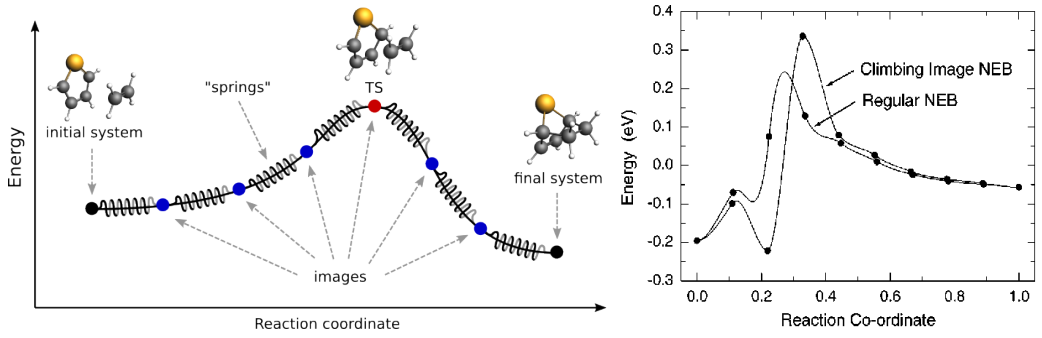

FIGURE 2.3: Schematic representation of NEB and difference between regular NEB and CI-NEB.

Thus, the image with highest energy will be made to converge to a saddle point and we will get a exact energy of the saddle point. Since the images in the band eventually converge to the MEP, they give a good approximation to the reaction coordinate around the saddle point, which gives an exact transition state of a reaction. Since all the images are being relaxed simultaneously, there is no additional cost of turning one of the images into a climbing image.

2.8 Computational and Visualization Packages

In this thesis, we used Quantum ESPRESSO (QE) simulation package which is an open-source computational software to perform electronic-structure calculations and material designing and modelling ranging from bulk to nano-scale[45, 46]. QE

is based on the formulation of density functional theory, pseudopotential methods and plane-wave approximation. We used QE package to perform *first-principles*

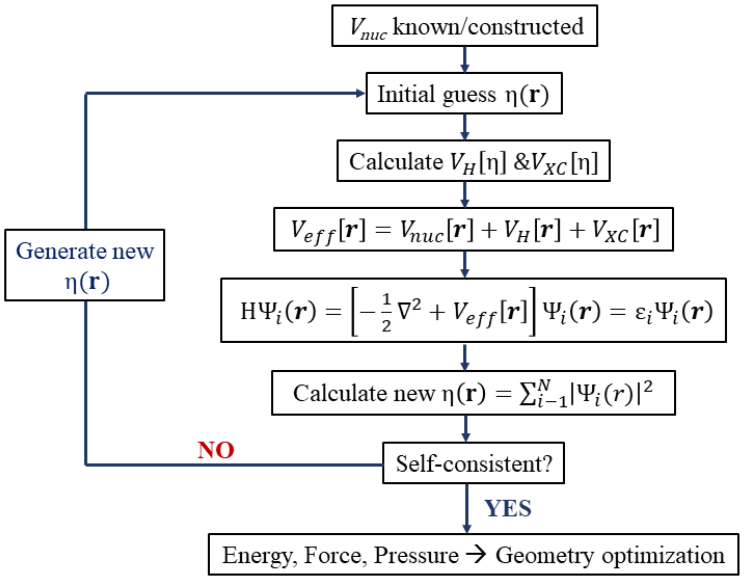

FIGURE 2.4: A typical self-consistency loop implemented in Quantum ESPRESSO code to compute the ground state of a material by solving the Kohn-Sham equations.

based computations under self-consistent field formalism, where it runs the self-consistency loop as shown in Fig. 2.4 to obtain the ground state energies of the considered systems. To compute and analyse the electronic structure, we performed the calculations in terms of non-self-consistent field formalism, wherein the computation of electronic eigen states as a function of crystal momentum. QE is such an all-round package that, we can use it to perform structural and geometric relaxations and optimizations, to compute the electronic properties of the system like band structure, density of states and orbital projected density of states. We can also incorporate van der Waals dispersion corrections in our study. The code also provides spin-polarized calculations which has great significance specially in case of metals and transition metals-based systems. Apart from this, we can analyse thermal, mechanical, vibrational, chemical and thermodynamical properties using this code.

As the software is open-source package, one can develop a code that can be interfaced with the QE easily to study and analyse the system in the way we want to do. For example, after obtaining ground state energies of the system by geometric optimization, we can analyse the adsorption mechanism of the considered system for particular reactants. Once we get an idea about the affinity of the system with the reactants, to actually perform the chemical reaction, a separate method

like climbing-image nudged elastic band (CI-NEB) method is implemented in QE package, which can give us an exact minimum energy path and reaction profile of a reaction just by providing the initial and final state of the reaction. In our calculations, we have used the CI-NEB method greatly to understand to reaction kinematics of various reactions.

In our study, to visualise the geometries of considered systems, to analyse the adsorption geometries and to plot and analyse various states of a reaction for particular reaction pathway, we used visualisation packages like XCrySDen and Vesta extensively[47, 48].

Bibliography

[1] E. Schrödinger. *Physical review*, 28(6):1049, 1926.

[2] J. C. Slater. *The Journal of Chemical Physics*, 41(10):3199–3204, 1964.

[3] D. S. Sholl and J. A. Steckel. Density functional theory, 2009.

[4] R. Eisberg and R. Resnick. *Quantum physics of atoms, molecules, solids, nuclei, and particles*. 1985.

[5] M. Born and R. Oppenheimer. *Annalen der Physik*, 389(20):457–484, 1927.

[6] C. A. Coulson. *Reviews of Modern Physics*, 32(2):170, 1960.

[7] D. R. Hartree. In *Mathematical Proceedings of the Cambridge Philosophical Society*, volume 24, pages 89–110. Cambridge university press, 1928.

[8] D. R. Hartree. In *Mathematical Proceedings of the Cambridge Philosophical Society*, volume 24, pages 111–132. Cambridge University Press, 1928.

[9] D. R. Hartree. In *Mathematical Proceedings of the Cambridge Philosophical Society*, volume 24, pages 426–437. Cambridge University Press, 1928.

[10] D. Hartree. In *Mathematical Proceedings of the Cambridge Philosophical Society*, volume 25, pages 310–314. Cambridge University Press, 1929.

[11] D. R. Hartree and W. Hartree. *Proceedings of the Royal Society of London. Series A-Mathematical and Physical Sciences*, 150(869):9–33, 1935.

[12] J. C. Slater. *Physical Review*, 32(3):339, 1928.

[13] J. C. Slater. *Physical review*, 36(1):57, 1930.

[14] V. Fock. *Zeitschrift für Physik*, 61:126–148, 1930.

[15] L. H. Thomas. In *Mathematical proceedings of the Cambridge philosophical society*, volume 23, pages 542–548. Cambridge University Press, 1927.

[16] E. Fermi. *Rend. Accad. Naz. Lincei*, 6(602-607):32, 1927.

[17] L. D. Hoffmann, G. L. Bradley and K. H. Rosen. *Calculus for business, economics, and the social and life sciences*. McGraw-Hill New York, USA, 1989.

[18] P. A. M. Dirac. *Proceedings of the Royal Society of London. Series A, Containing Papers of a Mathematical and Physical Character*, 133(821):60–72, 1931.

[19] C. v. Weizsäcker. *Zeitschrift für Physik*, 96(7):431–458, 1935.

[20] P. Hohenberg and W. Kohn. *Physical review*, 136(3B):B864, 1964.

[21] W. Kohn and L. J. Sham. *Physical review*, 140(4A):A1133, 1965.

[22] J. P. Perdew. *Physical Review Letters*, 55(16):1665, 1985.

[23] J. P. Perdew, K. Burke and M. Ernzerhof. *Physical review letters*, 77(18):3865, 1996.

[24] S. K. Ghosh and R. G. Parr. *Physical Review A*, 34(2):785, 1986.

[25] A. D. Becke and M. R. Roussel. *Physical Review A*, 39(8):3761, 1989.

[26] A. D. Becke. *The Journal of chemical physics*, 98(2):1372–1377, 1993.

[27] F. Bloch. *Zeitschrift für physik*, 52(7):555–600, 1929.

[28] M. Heideman, D. Johnson and C. Burrus. *IEEE Assp Magazine*, 1(4):14–21, 1984.

[29] M. C. Payne, M. P. Teter, D. C. Allan *et al. Reviews of modern physics*, 64(4):1045, 1992.

[30] D. Hamann, M. Schlüter and C. Chiang. *Physical review letters*, 43(20):1494, 1979.

[31] D. Vanderbilt. *Physical review B*, 41(11):7892, 1990.

[32] G. Kresse and D. Joubert. *Physical review b*, 59(3):1758, 1999.

[33] S. Grimme. *Journal of computational chemistry*, 25(12):1463–1473, 2004.

[34] S. Grimme. *Journal of computational chemistry*, 27(15):1787–1799, 2006.

[35] S. Grimme, J. Antony, S. Ehrlich *et al.* *The Journal of chemical physics*, 132(15), 2010.

[36] O. Jepson and O. Anderson. *Solid State Communications*, 9(20):1763–1767, 1971.

[37] P. E. Blöchl, O. Jepsen and O. K. Andersen. *Physical Review B*, 49(23):16223, 1994.

[38] M. Methfessel and A. Paxton. *physical review B*, 40(6):3616, 1989.

[39] T. Edvinsson. *Royal society open science*, 5(9):180387, 2018.

[40] B. Hammer and J. K. Nørskov. In *Advances in catalysis*, volume 45, pages 71–129. Elsevier, 2000.

[41] S. Bhattacharjee, U. V. Waghmare and S.-C. Lee. *Scientific reports*, 6(1):35916, 2016.

[42] H. Jónsson, G. Mills and K. W. Jacobsen. In *Classical and quantum dynamics in condensed phase simulations*, pages 385–404. World Scientific, 1998.

[43] G. Henkelman and H. Jónsson. *The Journal of chemical physics*, 113(22):9978–9985, 2000.

[44] G. Henkelman, B. P. Uberuaga and H. Jónsson. *The Journal of chemical physics*, 113(22):9901–9904, 2000.

[45] P. Giannozzi, S. Baroni, N. Bonini *et al.* *Journal of physics: Condensed matter*, 21(39):395502, 2009.

[46] P. Giannozzi, O. Andreussi, T. Brumme *et al.* *Journal of physics: Condensed matter*, 29(46):465901, 2017.

[47] A. Kokalj. *Journal of Molecular Graphics and Modelling*, 17(3-4):176–179, 1999.

[48] K. Momma and F. Izumi. *Journal of Applied crystallography*, 41(3):653–658, 2008.